Saudi Journal of Biological Sciences 29 (2022) 65–74

Contents lists available at ScienceDirect

Saudi Journal of Biological Sciences

journal homepage: www.sciencedirect.com

Original article

In silico analyses of major active constituents of fingerroot (*Boesenbergia rotunda*) unveils inhibitory activities against SARS-CoV-2 main protease enzyme

Arun Bahadur Gurung [a,*], Mohammad Ajmal Ali [b,*], Fahad Al-Hemaid [b], Mohamed El-Zaidy [b], Joongku Lee [c]

[a] Department of Basic Sciences and Social Sciences, North-Eastern Hill University, Shillong 793022, Meghalaya, India
[b] Department of Botany and Microbiology, College of Science, King Saud University, P.O. Box 2455, Riyadh 11451, Saudi Arabia
[c] Department of Environment and Forest Resources, Chungnam National University, 99 Daehak-ro, Yuseong-gu, Daejeon 34134, Republic of Korea

ARTICLE INFO

Article history:
Received 7 October 2021
Revised 14 November 2021
Accepted 22 November 2021
Available online 26 November 2021

Keywords:
Boesenbergia rotunda
SARS-CoV-2
Main protease inhibitors
COVID-19
Molecular docking
Molecular dynamics simulation
Alpinectin
Pinocembrin
Pinostrobin

ABSTRACT

Boesenbergia rotunda (L.) Mansf., commonly known as fingerroot is a perennial herb in the Zingiberaceae family with anticancer, anti-leptospiral, anti-inflammatory, antioxidant, antiulcer, and anti-herpes viral activities. While the severe acute respiratory syndrome coronavirus 2 (SARS-CoV-2) inhibitory activity of *B. rotunda* extract has been recently found, the active compounds contributing to this activity are yet unknown. The main protease (M^{pro}) enzyme is one of the most well established therapeutic targets among coronaviruses which plays a vital role in the maturation and cleavage of polyproteins during viral replication. The current work aims to identify active phytochemical substances from *B. rotunda* extract that can inhibit the replication of SARS-CoV-2 by using a combined molecular docking and dynamic simulation approaches. The virtual screening experiment revealed that fifteen molecules out of twenty-three major active compounds in the plant extract have acceptable drug-like characteristics. Alpinetin, Pinocembrin, and Pinostrobin have binding energies of −7.51 kcal/mol, −7.21 kcal/mol, and −7.18 kcal/mol, respectively, and can suppress M^{pro} activity. The stability of the simulated complexes of the lead compounds with the drug-receptor is demonstrated by 100-ns MD simulations. The binding free energies study utilizing molecular mechanics Poisson-Boltzmann surface area (MM-PBSA) and molecular mechanics generalized Born surface area (MM-GBSA) show that the compounds and M^{pro} enzyme have favourable thermodynamic interactions, which are majorly driven by van der Waals forces. Thus, the selected bioactive phytochemicals from *B. rotunda* might be used as anti-SARS-CoV-2 candidates that target the M^{pro} enzyme.

1. Introduction

Severe acute respiratory syndrome coronavirus 2 (SARS-CoV-2) is a highly contagious pathogen that appeared in late 2019 and is responsible for causing a global epidemic of acute respiratory sickness known as coronavirus disease 2019 (COVID-19) which has led to both a global health emergency and economic crisis (Hu et al., 2020). SARS-CoV-2 is a single-stranded, positive-sense, non-segmented enveloped RNA virus with a diameter of 50–200 nm and a size of 29.9 kb (Chen et al., 2020). It is a new betacoronavirus whose genomic sequence shares 79% similarity to severe acute respiratory syndrome coronavirus (SARS-CoV) and 50% similarity to Middle East respiratory syndrome coronavirus (MERS-CoV) (Lu et al., 2020). The genomic structure of SARS-CoV-2 is similar to that of other betacoronaviruses. The six functional open reading frames (ORFs) are replicase (ORF1a/ORF1b), spike (S), envelope (E), membrane (M), and nucleocapsid (N) in order from 5′ to 3′ (Hu et al., 2020). There are seven potential ORFs between the structural genes that encode accessory proteins (Chan et al., 2020). The replicase gene encodes a large polyprotein (pp1ab), which is proteolytically cleaved into 16 non-structural proteins (Nsps) involved in transcription and viral replication (Hu et al., 2020). The main protease (M^{pro}) or 3C-like protease ($3CL^{pro}$) or nsp5, a cysteine protease, is one of these Nsps which mediates the maturation and cleavage of polyproteins during viral replication (Ziebuhr

* Corresponding authors.
E-mail addresses: arunbgurung@gmail.com (A. Bahadur Gurung), alimohammad@ksu.edu.sa (M. Ajmal Ali).

Peer review under responsibility of King Saud University.

Production and hosting by Elsevier

https://doi.org/10.1016/j.sjbs.2021.11.053
1319-562X/

et al., 2000). The M^{pro} is a homodimer of three domains (domains I, II, and III) with a Cys-His catalytic dyad located in the cleft between domains I and II. Domains I and II are made up of six antiparallel β-barrels, with residues 8–101 and 102–184, respectively. Domain III (residues 201–303) is formed by an antiparallel globular cluster of five helices that is linked to domain II by a long loop (residues 185–200) (Mengist et al., 2021). The M^{pro} is one of the well-studied therapeutic targets among coronaviruses (Anand et al., 2003) and this enzyme, together with the papain-like protease(s), is required for the processing of polyproteins derived from viral RNA (Hilgenfeld, 2014). The M^{pro} cleaves the large polyprotein 1ab (replicase 1ab, 790 kDa) at 11 different location and the most common recognition sequence is Leu-Gln↓(Ser, Ala, Gly) (↓ marks the cleavage site). The SARS-CoV-2 replication can be stopped by inhibiting the activity of this enzyme target is inhibited and such inhibitors are unlikely to be harmful because no human proteases with similar cleavage selectivity are known (Zhang et al., 2020).

Boesenbergia rotunda (L.) Mansf. is a ginger species belonging to the Zingiberaceae family and grows in Southeast Asia, India, Sri Lanka, and Southern China (Eng-Chong et al., 2012). It is a perennial herb with a short stem that is replaced by pseudostems made up of leaf sheaths and can grow up to a height of 50 cm. There are 3–4 undivided, oval or elongate leaves that are 7–11 cm wide and 25–50 cm long. Rhizomes are light brown on the outside and yellow on the inside, ovoid-globose, and strongly aromatic (Ongwisespaiboon and Jiraungkoorskul, 2017). Developing from a central portion, the rhizomes resemble a bunch of fingers and therefore, it is commonly known as "fingerroot" in English (Eng-Chong et al., 2012). The plant is a rich source of various active phytochemical substances such as flavonoids, essential oils and polyphenols. *B. rotunda* rhizomes have been utilized as spices, flavouring agents, dyes, and traditional medicine (Ongwisespaiboon and Jiraungkoorskul, 2017). Some of the uses or phytochemical properties of *B. rotunda* include anti-allergic (Madaka et al., 2011), antibacterial (Udomthanadech et al., 2015; Zainin et al., 2013), anti-*Helicobacter pylori* (Bhamarapravati et al., 2006), anti-leptospiral (Chander et al., 2016), anticancer (Cheah et al., 2011), anti-inflammatory (Isa et al., 2012), antioxidant (Chiang et al., 2017), antiulcer (Abdelwahab et al., 2011), anti-dengue viral (Chee et al., 2010; Kiat et al., 2006) and anti-herpes viral activities (Wu et al., 2011) and wound healing (Mahmood et al., 2010). In Thailand, this plant is known as "Thai ginseng," and it is utilized as an aphrodisiac (Eng-Chong et al., 2012). More recently, the anti-SARS-CoV-2 activity of *Boesenbergia rotunda* extract and its bioactive compound, panduratin A has also been reported (Kanjanasirirat et al., 2020). In this present work, we have explored various bioactive compounds from *B. rotunda* extract as inhibitors of SARS-CoV-2 by targeting the main protease enzyme using molecular docking and dynamics approaches. We anticipate that the leads identified in the study can be used as potential inhibitors of SARS-CoV-2.

2. Materials and methods

2.1. Retrieval of ligands and structure optimization

A total of 23 active phytochemical substances present in *B. rotunda* extract belonging to different classes-flavonoids, essential oils, polyphenols and alkaloids were selected for the study (Ongwisespaiboon and Jiraungkoorskul, 2017). The three-dimensional structures of the compounds were obtained from the PubChem database (Kim et al., 2016). The structural optimization of the compounds was performed using the Merck molecular force field (MMFF94) (Halgren, 1996) and our previously published methodology (Gurung et al., 2016).

2.2. Virtual screening of drug-like molecules

The phytochemical substances were screened for drug-like properties based on physicochemical characteristics specified by Lipinski's rule of five (ROF) (Lipinski, 2004) and Veber's rule (Veber et al., 2002) filters. The DataWarrior program version 4.6.1 was used to determine the physicochemical characteristics of the compounds (Sander et al., 2015).

2.3. Retrieval and preparation of target enzyme

The three-dimensional structure of the target enzyme M^{pro} was obtained from protein data bank (PDB) using accession ID 7L0D. The X-ray crystal structure has been resolved at a resolution of 2.39 Å containing the SARS-CoV-2 Main protease (M^{pro}) complexed with an inhibitor ML188 (Lockbaum et al., 2021). The heteroatoms, including ions, co-crystallized ligand and water molecules, were removed from the target enzyme. AutoDock Tools-1.5.6 tool (Morris et al., 2009) was used for adding a suitable number of polar hydrogen atoms and Kolmann charges to the target enzyme.

2.4. Preparation of ligands

Each ligand molecule was prepared for molecular docking by the addition of Gasteiger charges and hydrogen atoms and optimally defined torsions using AutoDock Tools-1.5.6 (Morris et al., 2009).

2.5. Molecular docking validation

A redocking experiment was performed using the co-crystal compound to see if the molecular docking parameters and method could accurately replicate the natural binding poses.

2.6. Molecular docking

The Lamarckian genetic algorithm was employed for molecular docking experiments where the docking parameters were selected from our previously reported methodology (Gurung et al., 2016). AutoDock4.2 software was used to perform molecular docking (Morris et al., 2009). The binding site of the compounds was defined by choosing a grid box centred at the cocrystal ligand with xyz coordinates of 11.476, −1.396 and 21.127, number of grid points of 60 × 60 × 60 and grid spacing of 0.375 Å. For each compound, a total of fifty separate docking runs were performed. The docking poses were conformationally clustered using a root mean square deviation (RMSD) cut-off value of 2.0 Å. The most favourable binding poses of the compounds were explored by determining the lowest binding free energy (ΔG) using the equation (**Eq. (1)**):

$$\Delta G = \Delta G_{vdw}\sum_{i,j}\left(\frac{A_{ij}}{r_{ij}^{12}}-\frac{B_{ij}}{r_{ij}^{6}}\right)+\Delta G_{hbond}\sum_{i,j}\left(E(t)\frac{C_{ij}}{r_{ij}^{12}}-\frac{D_{ij}}{r_{ij}^{10}}+E_{hbond}\right) +\Delta G_{eiec}\sum_{i,j}\frac{q_i q_j}{\varepsilon(r_{ij})r_{ij}}+\Delta G_{tor}N_{tor}+\Delta G_{desolv}\sum_{iC,j}\left(S_i V_j e^{(-\eta ij^2/2\sigma^2)}\right) \quad (1)$$

Where ΔG_{vdw} the van der Waals energy, ΔG_{hbond} the Hydrogen Bonding energy, ΔG_{elec} the Electrostatics energyΔG_{tor} the Torsional free energy change and ΔG_{desolv} the Desolvation energy

The inhibition constant (K_i) of the compounds was calculated using the following equation (**Eq. (2)**)

$$K_i = exponential\ (\Delta G/RT) \quad (2)$$

ΔG is the binding energy in kcal/mol, R is the universal gas constant (1.987 $calK^{-1}$ mol^{-1}), and T is the temperature (298.15 K).

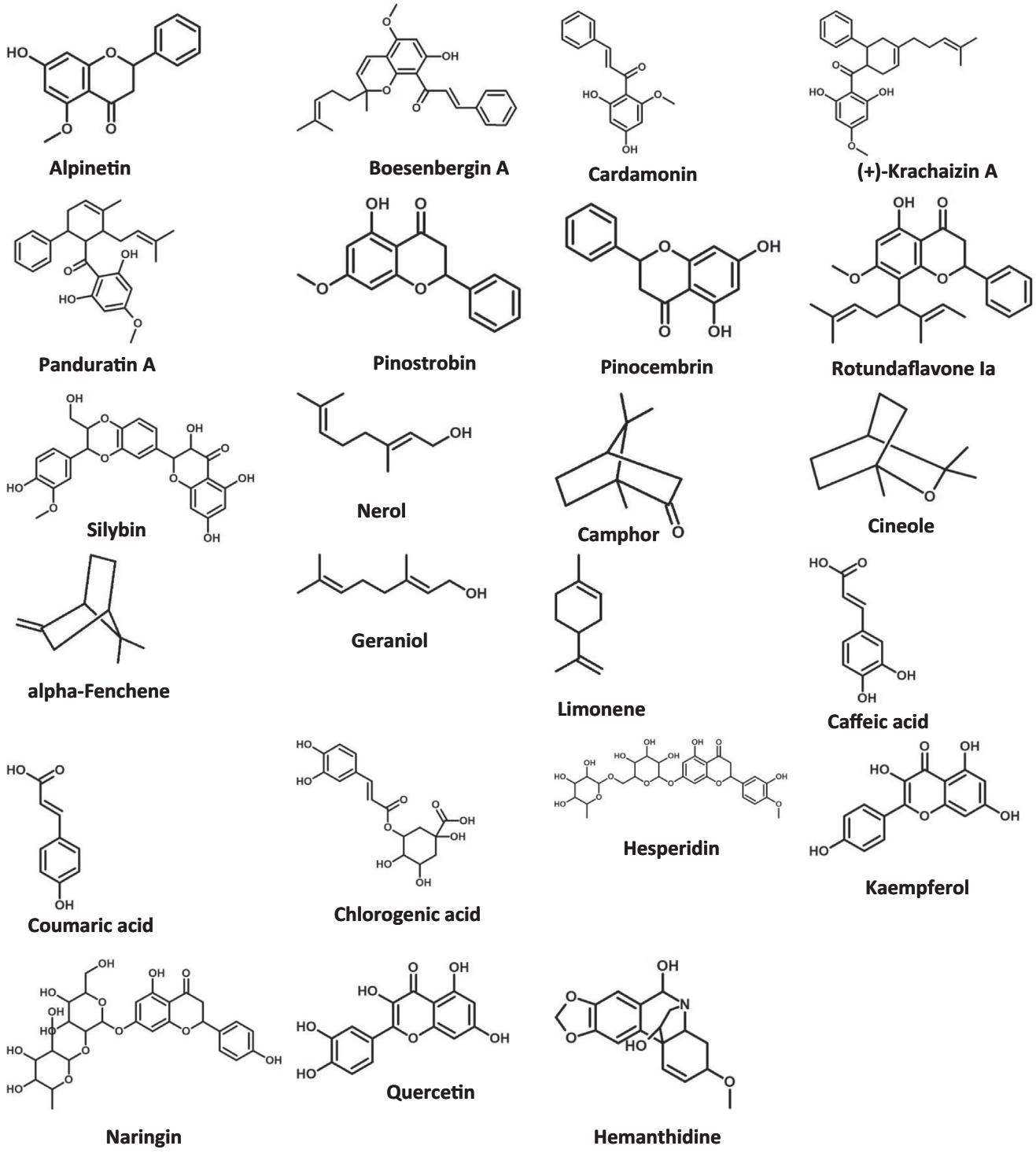

Fig. 1. Bioactive compounds from *B. rotunda* extract selected for virtual screening process.

The hydrogen bonds and hydrophobic interactions between the compounds and the target enzyme were investigated using LigPlot + v 1.4.5 (Laskowski and Swindells, 2011).

2.7. MM/PBSA energy calculation

The ligand and receptor molecular dynamics (LARMD) was used to determine the binding free energies (ΔG_{bind}) between the compound and the target enzyme using the following (**Eq. (3)**)

$$\Delta G_{bind} = \Delta E_{bind} - T\Delta S_{sol} - T\Delta S_{conf} \quad (3)$$

$T\Delta S_{sol}$ is the solvation entropy, and $T\Delta S_{conf}$ is the conformational entropy, where ΔE_{bind} is the binding energy and $T\Delta S_{conf}$ is the conformational entropy. The entropy was calculated using an empirical approach (Hao et al., 2009; Pan et al., 2008), and the enthalpy was determined using the MM/PB (GB) SA technique (Hou et al., 2011).

2.8. MD simulation studies

100-ns MD simulations were performed on the unbound SARS-CoV-2 M^{pro} and M^{pro}-ligand docked complexes using GROningen MAchine for Chemical Simulations (GROMACS) 2019.2 software

Table 1
Physicochemical characteristics of the compounds. The grey highlighted rows indicate the compounds obeying the Lipinski's rule of five and Veber's rule criteria.

Molecule Name	CID	MW	LogP	HBA	HBD	TPSA	RB
Alpinetin	154,279	270.283	2.7771	4	1	55.76	2
Boesenbergin A	6,313,827	404.504	6.0866	4	1	55.76	7
Cardamonin	641,785	270.283	2.5424	4	2	66.76	4
(+)-Krachaizin A	11,729,201	406.52	6.1945	4	2	66.76	7
Panduratin A	6,483,648	406.52	6.0094	4	2	66.76	6
Pinostrobin	73,201	270.283	2.7771	4	1	55.76	2
Pinocembrin	68,071	256.256	2.5014	4	2	66.76	1
Rotundaflavone Ia	101,863,268	406.52	6.9445	4	1	55.76	6
Silybin	3,086,637	482.44	2.1266	10	5	155.14	4
Nerol	643,820	154.252	3.4853	1	1	20.23	4
Camphor	2537	152.236	2.1793	1	0	17.07	0
Cineole	2758	154.252	2.1095	1	0	9.23	0
alpha-Fenchene	28,930	136.237	2.7993	0	0	0	0
Geraniol	637,566	154.252	3.4853	1	1	20.23	4
Limonene	22,311	136.237	3.3614	0	0	0	1
Caffeic acid	689,043	180.159	0.7825	4	3	77.76	2
Coumaric acid	637,542	164.16	1.1282	3	2	57.53	2
Chlorogenic-acid	1,794,427	354.31	−0.7685	9	6	164.75	5
Hesperidin	10,621	610.563	−0.814	15	8	234.29	7
Kaempferol	5,280,863	286.238	1.8359	6	4	107.22	1
Naringin	442,428	580.537	−0.744	14	8	225.06	6
Quercetin	5,280,343	302.237	1.4902	7	5	127.45	1
Hemanthidine	3,002,914	317.34	0.7421	6	2	71.39	1

program (Hess et al., 2008) with the GROMOS96 43a1 force field. The systems were solvated in a water-filled 3-D cube with 1 Å spacing using a three-point model for water called simple point charge (SPC216). Newton's equations of motion were integrated using a leap-frog temporal integration technique. The systems were subjected to neutralization, and the amount of energy was optimized. The temperature was set to 300 K, and the systems were equilibrated for 300 ps in the NVT ensemble (Number of particles, Volume, and Temperature) and another 300 ps in the NPT ensemble (Number of particles, Volume, and Temperature) (Number of particles, Pressure and Temperature). The systems were submitted to a production MD run in NPT ensemble for 100 ns after heating and equilibration. The topologies of ligands compatible with the GROMOS96 43a1 force field were generated using the PRODRG web server (Schüttelkopf and Van Aalten, 2004). The Xmgrace plotting tools were used to generate the graphs.

3. Results

A total of 23 major active phytochemical substances from *B. rotunda* extracts were chosen for the study. The phytochemical set consists of nine numbers of flavonoids including Alpinetin (CID154279), Boesenbergin A (CID6313827), Cardamonin (CID641785), (+)-Krachaizin A (11729201), Panduratin A (CID6483648), Pinostrobin (CID73201), Pinocembrin (CID68071), Rotundaflavone Ia (CID101863268) and Silybin (CID3086637), six numbers of essential oils including Nerol (CID643820), Camphor (CID2537), Cineole (CID2758), alpha-Fenchene (CID28930), Geraniol (CID637566) and Limonene (CID22311) and seven numbers of polyphenols including Caffeic acid (CID689043), Coumaric acid (CID637542), Chlorogenic-acid (CID1794427), Hesperidin (CID10621), Kaempferol (CID5280863), Naringin (CID442428) and Quercetin (CID5280343) and one alkaloid- Hemanthidine (CID3002914). The three-dimensional structures of the optimized compounds used for virtual screening and molecular docking investigations are depicted in Fig. 1.

Out of a total of 23 phytochemicals, 5 flavonoids (Alpinetin, Cardamonin, Geraniol, Pinostrobin and Pinocembrin), 5 essential oils (Nerol, Camphor, Cineole, alpha-Fenchene, Hemanthidine and Limonene), 4 polyphenols (Caffeic acid, Coumaric acid, Kaempferol and Quercetin) and 1 alkaloid (Hemanthidine) were found to be orally bioavailable according to Lipinski's rule of five-(Molecular weight (MW) $\leq$ 500, LogP (partition coefficient between n-octanol and water) $\leq$ 5, number of hydrogen bond donors (HBD) $\leq$ 5 and number of hydrogen bond acceptors (HBA) $\leq$ 10 [23]) and Veber's rule-(rotatable bond count (RB) $\leq$ 10 and topological polar surface area (TPSA) $\leq$ 140 Å^2) (Table 1). These drug-like molecules were then used in molecular docking experiments.

The redocking experiment with the co-crystal compound (ML188) verified the molecular docking procedure and algorithm. The RMSD of the docked and native co-crystal positions was found to be 0.981 Å (Fig. 2). This modest difference (RMSD < 2.0 Å) sug-

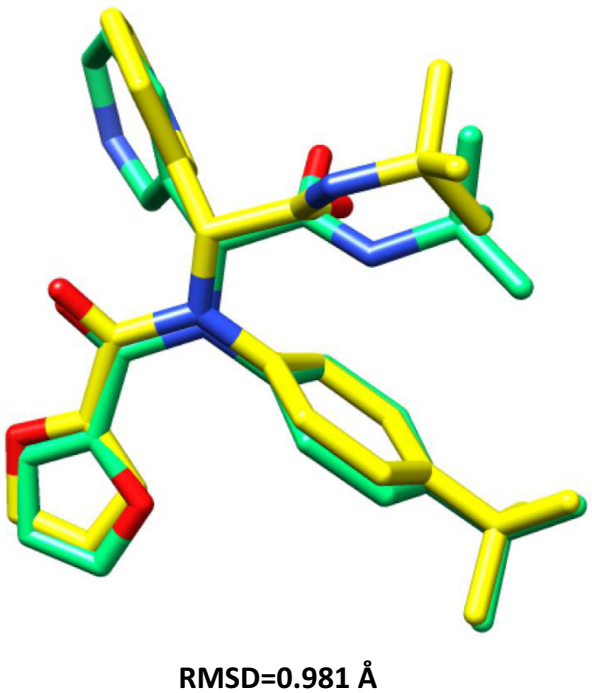

Fig. 2. Molecular docking validation. The superposition of the native crystal pose (yellow) on docked pose (spring green) of the cocrystal ligand (ML188). For clarity, the hydrogen atoms are not depicted in the figure.

Table 2
Binding energies and inhibition constant of the selected compounds.

Compounds	CID	Molecular formula	Binding Energy (kcal/mol)	Inhibition constant (μM)
Alpinetin	154,279	C16H14O4	−7.51	3.12
Cardamonin	641,785	C16H14O4	−7.09	6.31
Pinostrobin	73,201	C16H14O4	−7.18	5.47
Pinocembrin	68,071	C15H12O4	−7.21	5.21
Nerol	643,820	C10H18O	−5.39	111.16
Camphor	2537	C10H16O	−5.32	125.41
Cineole	2758	C10H18O	−5.41	107.78
α-Fenchene	28,930	C10H16	−5.28	135.59
Geraniol	637,566	C10H18O	−5.27	136.65
Limonene	22,311	C10H16	−4.83	287.01
Caffeic acid	689,043	C9H8O4	−4.92	247.62
Coumaric acid	637,542	C9H8O3	−4.59	429.66
Kaempferol	5,280,863	C15H10O6	−6.91	8.62
Quercetin	5,280,343	C15H10O7	−7.07	6.53
Hemanthidine	3,002,914	C17H19NO5	−6.99	7.46
0EN	–	C26H31N3O3	−8.7	0.41627

gests that the docking methods and parameters employed in the study are capable of correctly predicting the native conformations of the compounds.

The fifteen selected drug-like small molecules were docked into the active site pocket of SARS-CoV-2 M^{pro}. The binding energies and the inhibition constants of the docked molecules derived from molecular docking results are shown in Table 2. The best-ranked lead molecule i.e., Alpinetin shows binding energy of −7.51 kcal/mol and an inhibition constant of 3.12 μM when it interacts with the target enzyme. Alpinetin establishes one hydrogen bond with Gln192 of bond length 3.14 Å and hydrophobic interactions with eleven residues (His41, Met49, Tyr54, Met165, Glu166, Leu167, Pro168, Asp187, Arg188, Gln189 and Thr190) (Fig. 3**A**). The second lead molecule i.e., Pinocembrin interacts with the target enzyme with a binding energy of −7.21 kcal/mol and an inhibition constant of 5.21 μM. This interaction is strengthened by the establishment of one hydrogen bond with Thr190 of hydrogen bond length of 2.58 Å and with the involvement of nine residues (His41, Met49, Tyr54, Met165, Glu166, Pro168, Asp187, Arg188 and Gln189) contributing to hydrophobic interactions (Fig. 3**B**). The third lead molecule- Pinostrobin interacts with SARS-CoV-2 M^{pro} with a binding energy of −7.18 kcal/mol and an inhibition constant of 5.47 μM. The molecular interaction is facilitated through one hydrogen bond with Glu166 of hydrogen bond length 3.25 Å and hydrophobic interactions via eleven residues (His41, Cys44, Met49, Tyr54, His164, Met165, Pro168, Asp187, Arg188, Gln189 and Thr190) (Fig. 3**C**). The standard inhibitor ML188 interacts with SARS-CoV-2 M^{pro} with a binding energy of −8.70 kcal/mol and an inhibition constant of 0.416 μM. The binding interaction is mediated through three hydrogen bonds with His163 of bond length 3.03 Å, Ser144 of bond length 2.83 Å, Gly143 with a bond length of 3.15 Å and Glu166 of bond length of 3.02 Å, and hydrophobic interactions via fourteen residues (Thr25, Thr26, Leu27, His41, Met49, Phe140, Leu141, Asn142, Cys145, His164, Met165, Asp187, Arg188 and Gln189) (Fig. 3**D**).

The unbound M^{pro} and its complexes with the top 3 ranked compounds- Alpinetin, Pinocembrin, Pinostrobin and the cocrystal compound (ML188) were subjected to MD simulations for 100 ns and various structural properties were derived from their trajectories (Table 3). The root-mean-square deviation (RMSD) is a useful parameter for evaluating the structural deviation of atomic positions and stability in protein structures (**Eq. (4)**).

$$RMSD(t_1,t_2)=\left[\frac{1}{M}\sum_{i=1}^{N}m_i\| r_i(t_1)-r_i(t_2)\|^2\right]^{1/2} \quad (4)$$

Where $M=\sum_{i=1}^{N}m_i$ and $r_i(t_i)$ the position of atom i at time t **(4)**

M^{pro}, M^{pro}_Alpinetin, M^{pro}_Pinocembrin, M^{pro}_Pinostrobin and M^{pro}_ ML188 complexes have an average RMSD of 0.280311 ± 0.0 32395 nm, 0.334146 ± 0.030096 nm, 0.322419 ± 0.04002 nm, 0.3 33004 ± 0.038473 nm and 0.308355 ± 0.045476 nm respectively (Table 3). According to the RMSD plot, the binding of the compounds causes an enhancement in the structural flexibility of the target enzyme (Fig. 4). The average RMSD values of Alpinetin, Pinocembrin, Pinostrobin and ML188 were 0.717544 ± 0.149986 n m, 0.38543 ± 0.084949 nm, 0.332535 ± 0.067798 nm and 0.2938 73 ± 0.058403 nm and the subtle variations in the RMSD indicate that the compounds have favourable binding orientations in the binding pocket of the target enzyme. An average of the residual fluctuations in SARS-CoV-2 M^{pro} was computed (**Eq. (5)**) and plotted as the root-mean-square fluctuation (RMSF) to study the local fluctuations in the target enzyme before and after binding of compounds. (Fig. 5).

$$RMSD_i=\left[\frac{1}{T}\sum_{t_j=1}^{T}\| r_i(t_j)-r_i^{ref}\|^2\right]^{1/2} \quad (5)$$

Where T is the time span over which the average to be calculated, and r_i^{ref} the particle i's reference location.

The RMSF figure revealed multiple residual variations in several positions in the target enzyme with residues Leu50 (0.6964 nm), Asn51 (0.6041 nm), Gly302 (0.5032 nm), Val303 (0.5732 nm), Thr304 (0.6642 nm) and Phe305 (0.8111 nm) experiencing greater than 0.5 nm amplitudes of fluctuations. The radius of gyration (Rg) is a metric that is directly linked to a protein's overall structural shape and is used to deduce protein stability and folding behaviour (**Eq. (6)**).

$$R_g=\left(\frac{\sum_i\| r_i\|^2 m_i}{\sum_i m_i}\right)^{1/2} \quad (6)$$

Where m_i Is the mass of atom i and r_i is the position of atom i with respect to the centre of mass of the molecule.

The Rg of unbound M^{pro} and M^{pro} docked complexes were calculated to determine their structural compactness (Fig. 6). The Rg values for M^{pro}, M^{pro}_Alpinetin, M^{pro}_Pinocembrin, M^{pro}_Pinostrobin and M^{pro}_ ML188 complexes were 2.127997 ± 0.021204 n m, 2.085232 ± 0.021426 nm, 2.08275 ± 0.01947 nm, 2.082476 ± 0. 019272 nm and 2.107948 ± 0.01986 nm respectively. When compared to free M^{pro}, the complexes have a slightly lower Rg and maintains a stable equilibrium after 30 ns. In this case, the Rg plot analysis suggests that M^{pro} undergoes conformational changes resulting in increased structural compactness with the binding of the compounds. A protein's solvent accessible surface area (SASA)

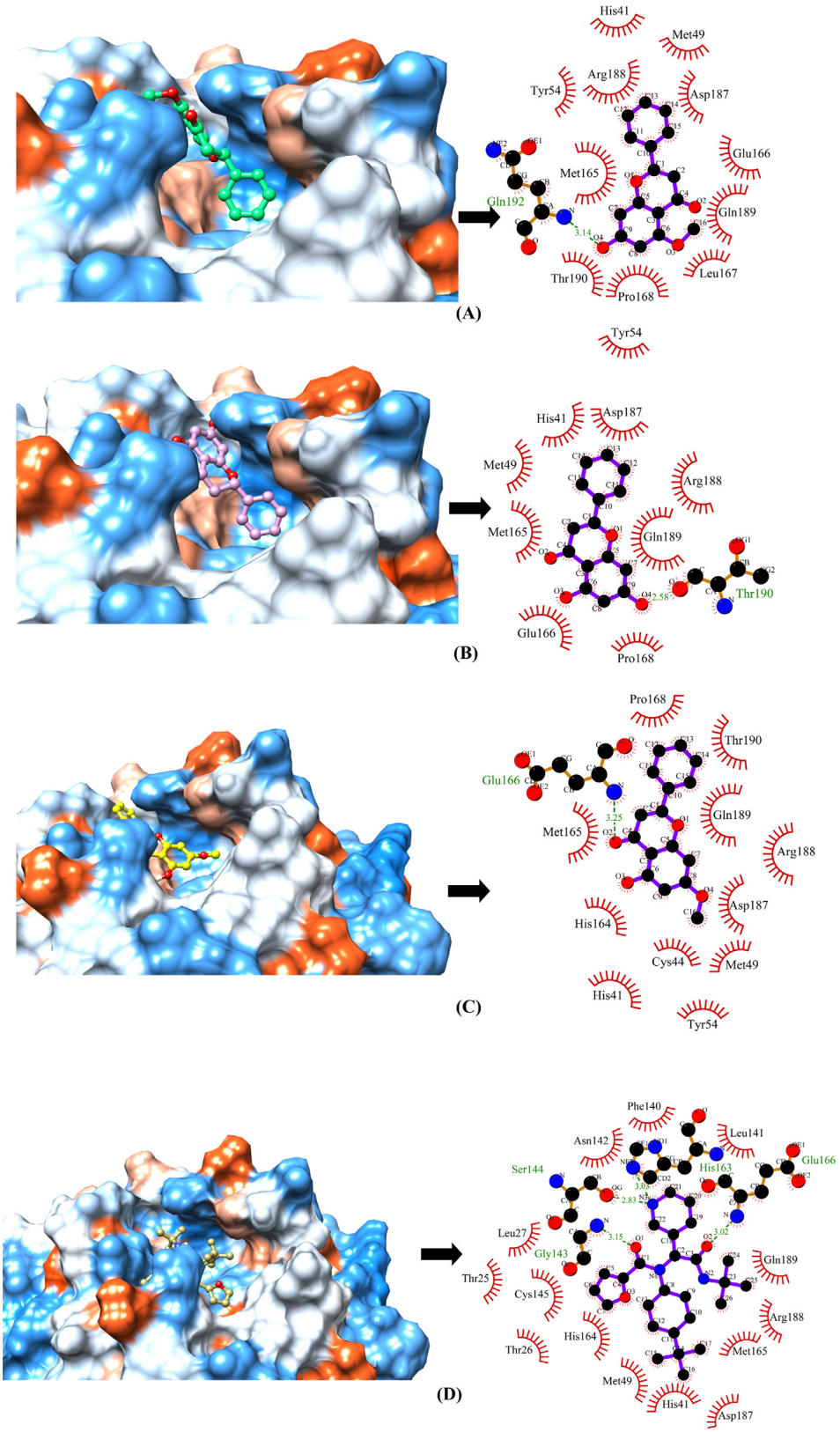

Fig. 3. The hydrophobic surface view of the binding pocket and molecular interactions between SARS-CoV-2 and compounds (A) Alpinetin (B) Pinocembrin (C) Pinostrobin (CID11531457) (D) control (ML188). The Kyte-Doolittle scale has been used to depict hydrophobicity, with dodger blue being the most hydrophilic, white being neutral and orange red representing the most hydrophobic. Hydrogen bonds are shown by green dashed lines, whereas hydrophobic interactions are represented by red arcs. The ligands are coloured blue, whereas important protein residues are coloured black (hydrophobic) or red (hydrogen bonds).

Table 3
Average structural properties of unbound SARS-CoV-2 M^{pro} and SARS-CoV-2 docked complexes.

Systems	RMSD (nm)		Rg (nm)	Total SASA (nm^2)	Hydrogen bonds	
	Protein	Ligand			Protein	Ligand
M^{pro}	0.280311± 0.032395	–	2.127997± 0.021204	128.3938± 6.842137	215.2897± 8.083191	–
M^{pro}_Alpinetin	0.334146± 0.030096	0.717544± 0.149986	2.085232± 0.021426	128.3513± 7.047367	217.3377± 8.293122	0.41958± 0.579462
M^{pro}_Pinocembrin	0.322419± 0.04002	0.38543± 0.084949	2.08275± 0.01947	128.2853± 4.886376	215.3976± 8.299262	0.612388± 0.727741
M^{pro} _Pinostrobin	0.333004± 0.038473	0.332535± 0.067798	2.082476± 0.019272	126.8495± 6.501256	211.3786± 8.336636	0.436563± 0.525568
M^{pro} _0EN	0.308355± 0.045476	0.293873± 0.058403	2.107948± 0.01986	130.6634± 5.435755	214.8142± 7.892619	0.757816

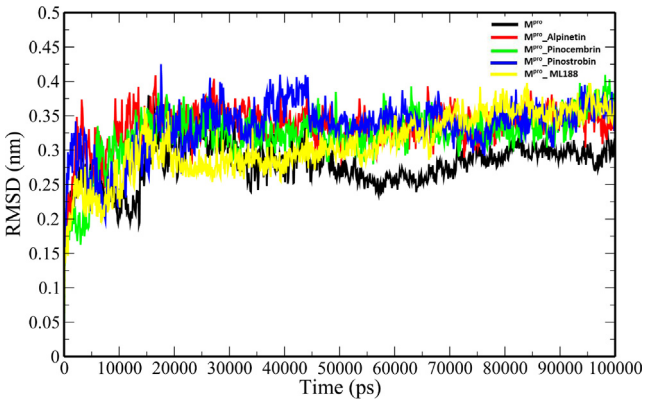

Fig. 4. RMSD plot of backbone atoms of unbound SARS-CoV-2 M^{pro} and SARS-CoV-2 M^{pro} docked complexes.

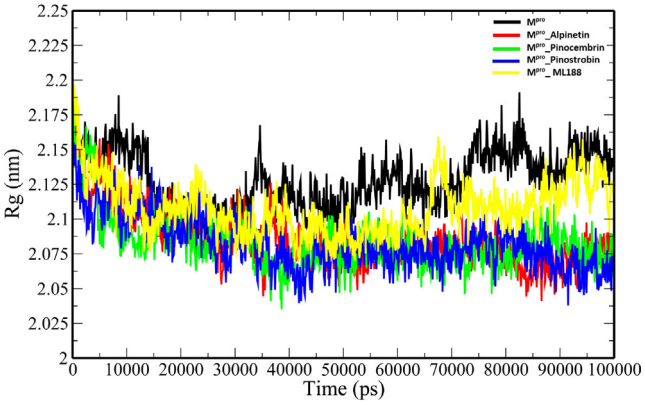

Fig. 6. Rg plot of unbound SARS-CoV-2 M^{pro} and SARS-CoV-2 M^{pro} docked complexes.

is the region of the protein that interacts directly with its surrounding solvent molecules. During the 100 ns MD simulation, the SASA plot for unbound SARS-CoV-2 M^{pro} and SARS-CoV-2 M^{pro} docked complexes were generated (Fig. 7). The average SASA values for M^{pro}, M^{pro}_Alpinetin, M^{pro}_Pinocembrin, M^{pro}_Pinostrobin and M^{pro}_ML188 complexes were determined to be 128.3938 ± 6. 842137 nm^2, 128.3513 ± 7.047367 nm^2, 128.2853 ± 4.886376 n m^2, 126.8495 ± 6.501256 nm^2 and 130.6634 ± 5.435755 nm^2 respectively. After interaction with the compounds except for ML188, a modest decrease in SASA was detected due to the conformational changes in the protein. A protein's stability and overall shape are dependent on intramolecular hydrogen bonding. Hydrogen bonds formed during the simulation were computed and displayed to confirm the stability of unbound SARS-CoV-2 M^{pro} and SARS-CoV-2 M^{pro} docked complexes (Fig. 8**A**). The average number of intramolecular hydrogen bonds in M^{pro}, M^{pro}_Alpinetin, M^{pro}_-Pinocembrin, M^{pro}_Pinostrobin and M^{pro}_ML188 complexes were 215.2897 ± 8.083191, 217.3377 ± 8.293122, 215.3976 ± 8.299262 , 211.3786 ± 8.336636, 214.8142 ± 7.892619 respectively. The average number of hydrogen bonds displayed by the compounds-Alpinetin, Pinocembrin, Pinostrobin and the cocrystal compound (ML188) were 0.41958 ± 0.579462, 0.612388 ± 0.727741, 0.4365

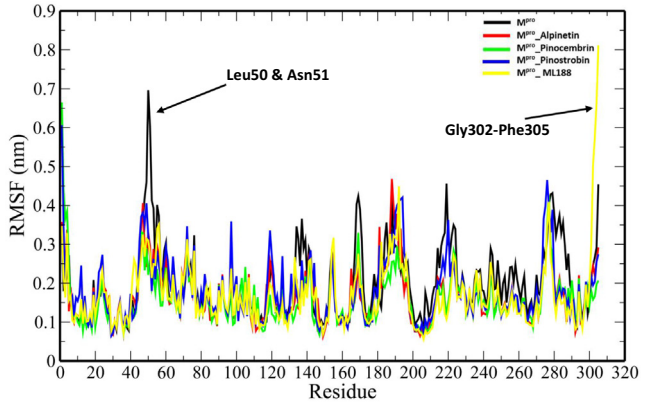

Fig. 5. RMSF analysis of unbound SARS-CoV-2 M^{pro} and SARS-CoV-2 M^{pro} docked complexes with the labelled residues depicting high amplitude of fluctuations.

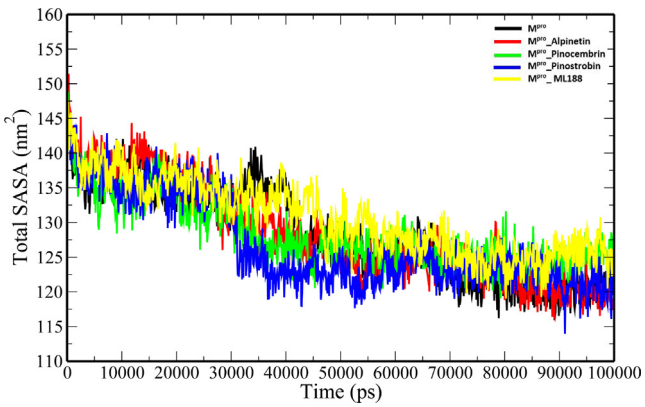

Fig. 7. Total SASA plot of unbound SARS-CoV-2 M^{pro} and SARS-CoV-2 M^{pro} docked complexes,

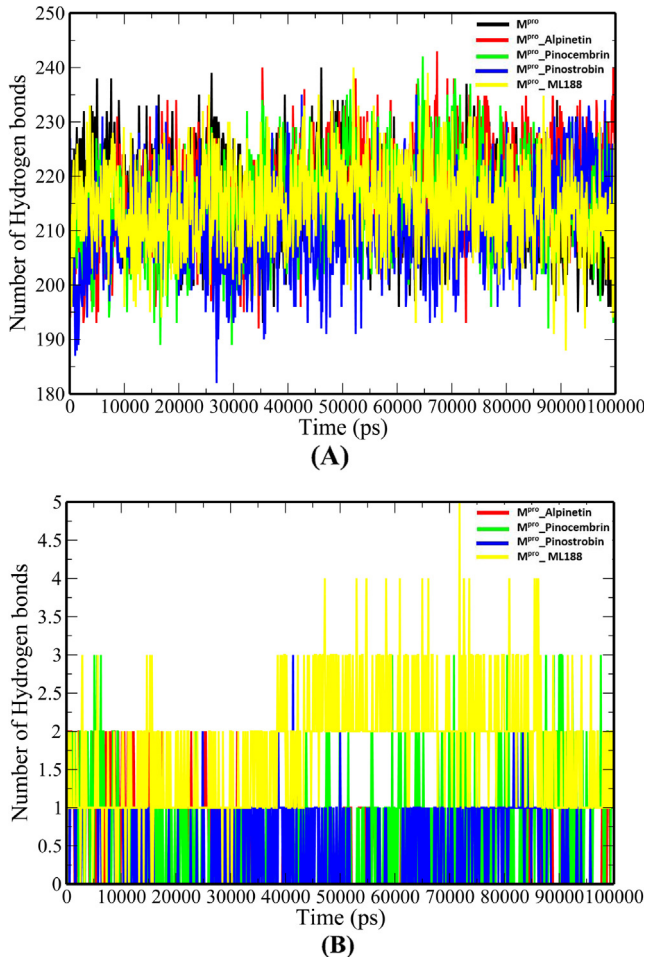

Fig. 8. Plot of Number of hydrogen bonds-(A) intraprotein (B) M^{pro} and compounds.

63 ± 0.525568 and 1.714286 ± 0.757816 respectively which help to stabilize the protein–ligand complexes (Fig. 8**B**).

Molecular mechanics Poisson–Boltzmann surface area (MM-PBSA) and molecular mechanics generalized Born surface area (MM-GBSA) methods were used to evaluate the binding free energies of the compounds-Alpinetin (ΔPB = −3.61 kcal/mol, ΔGB = −8.45 kcal/mol), Pinocembrin (ΔPB = −6.40 kcal/mol, ΔGB = −10.05 kcal/mol), Pinostrobin (ΔPB = −6.23 kcal/mol, ΔGB = −10.13 kcal/mol) and the control (ML188) (ΔPB = −15.23 kcal/mol, ΔGB = −19.97 kcal/mol) (Table 4). The Gas phase and van der Waals energy make a significant contribution to the binding free energy. The major residues contributing towards the binding interaction between Alpinetin and M^{pro} include Met165 (−1.87 kcal/mol), Gln189 (−1.81 kcal/mol), Met49 (−1.28 kcal/mol), Gln192 (−0.85 kcal/mol), Pro168 (−0.84 kcal/mol), Asp187 (−0.79 kcal/mol), Leu167 (−0.71 kcal/mol), Thr190 (−0.7 kcal/mol), His41 (−0.68 kcal/mol) and Arg188 (−0.57 kcal/mol) (Fig. 9**A**). In case of M^{pro}_Pinocembrin complex, residues such as Met165 (−2.9 kcal/mol), Gln189 (−2.21 kcal/mol), Met49 (−1.65 kcal/mol), His41 (−1.49 kcal/mol), Pro168 (−1.26 kcal/mol), Leu167 (−0.61 kcal/mol), Arg188 (−0.59 kcal/mol), Asp187 (−0.36 kcal/mol), Gln192 (−0.36 kcal/mol), Thr190 (−0.33 kcal/mol) contribute majorly to the total binding energy (Fig. 9**B**). The top ten residues contributing towards the binding interaction between Pinostrobin and M^{pro} include Met165 (−1.79 kcal/mol), Gln189 (−1.79 kcal/mol), Thr190 (−1.35 kcal/mol), Ala191 (−0.99 kcal/mol), Gln192 (−0.95 kcal/mol), Leu167 (−0.89 kcal/mol), Pro168 (−0.75 kcal/mol), Arg188 (−0.47 kcal/mol), His41 (−0.43 kcal/mol) and Val186 (−0.24 kcal/mol) (Fig. 9**C**). In case of M^{pro}_ ML188 complex, residues such as Met165 (−3.07 kcal/mol), Glu166 (−1.6 kcal/mol), Cys145 (−1.56 kcal/mol), His41 (−1.44 kcal/mol), Asn142 (−1.24 kcal/mol), Met49 (−1.17 kcal/mol), Gly143 (−0.73 kcal/mol), Leu27 (−0.67 kcal/mol), Gln189 (0.5 kcal/mol) and Asp187 (−0.47 kcal/mol) have higher contribution toward the total binding energy (Fig. 9**D**).

4. Discussion

The SARS-CoV-2 main protease (M^{pro}) enzyme is a druggable target for COVID-19, a fatal disease for which there are currently no effective drugs available. The main protease (M^{pro}) also known as 3C-like protease (3CLpro) or nsp5 is a cysteine protease that plays a key role in the maturation and cleavage of polyproteins during viral replication (Ziebuhr et al., 2000). The enzyme is a homodimer with three domains (domains I, II, and III) and a Cys-His catalytic dyad in the cleft between domains I and II. Inhibition of this essential enzyme using small molecules may be an effective strategy to halt the virus replication cycle. Plants have been in use for many centuries as an effective source of antiviral molecules used against different types of viral diseases. The recently identified anti-SARS-CoV-2 activity of the extract and phytochemical component, panduratin A from the perennial herb, *Boesenbergia rotunda* (L.) Mansf. (Kanjanasirirat et al., 2020) draws the attention of the researchers to explore this plant's phytochemicals against COVID-19. *B. rotuda* commonly known as "fingerroot" in English is a ginger species belonging to the Zingiberaceae family (Eng-Chong et al., 2012). In the present study, we used a high-resolution experimental structure of SARS-CoV-2 Main protease enzyme in complex with ML188 for structure-based identification of non-covalent inhibitors from *B. rotunda* extract. ML188 is a non-covalent inhibitor that inhibits SARS-CoV-M^{pro} with an IC_{50} of 4.5 ± 0.5 μM and inhibits SARS-CoV-2-M^{pro} with an IC_{50} of 2.5 ± 0.3 μ

Table 4
Evaluations of binding free energy between the compounds and SARS-CoV-2 M^{pro}.

Protein-ligand complexes	ELE[1]	VDW[2]	GAS[3]	PBSOL[4]	PBTOT[5]	GBSOL[4]	GBTOT[5]	-TS[6]	$\triangle G_{PB}$[7]	$\triangle G_{GB}$[7]
M^{pro}_Alpinetin	−4.08 ± 3.21	−35.43 ± 3.36	−39.51 ± 5.18	14.85 ± 2.76	−24.66 ± 3.32	10.01 ± 2.14	−29.50 ± 3.64	21.05 ± 2.63	−3.61	−8.45
M^{pro}_Pinocembrin	−4.32 ± 1.77	−30.92 ± 1.91	−35.25 ± 2.64	13.21 ± 1.65	−22.04 ± 2.39	9.56 ± 1.36	−25.69 ± 2.01	15.64 ± 1.28	−6.40	−10.05
M^{pro} _Pinostrobin	−4.17 ± 2.15	−36.84 ± 2.09	−41.01 ± 3.04	13.69 ± 1.98	−27.33 ± 2.45	9.78 ± 1.68	−31.23 ± 2.13	21.10 ± 1.32	−6.23	−10.13
M^{pro} _0EN	−7.70 ± 1.64	−50.46 ± 2.54	−58.15 ± 3.03	19.82 ± 1.86	−38.33 ± 2.87	15.08 ± 1.41	−43.07 ± 2.45	23.10 ± 1.51	−15.23	−19.97

[1] Electrostatic energy as calculated by the MM force field;
[2] Van der Waals contribution from MM;
[3] Total gas-phase energy;
[4] Non-polar and polar contributions to solvation based on PB/GB model;
[5] Final estimated binding free energy calculated from GAS and PBSOL/GBSOL;
[6] Entropy;
[7] Binding free energy with entropy.

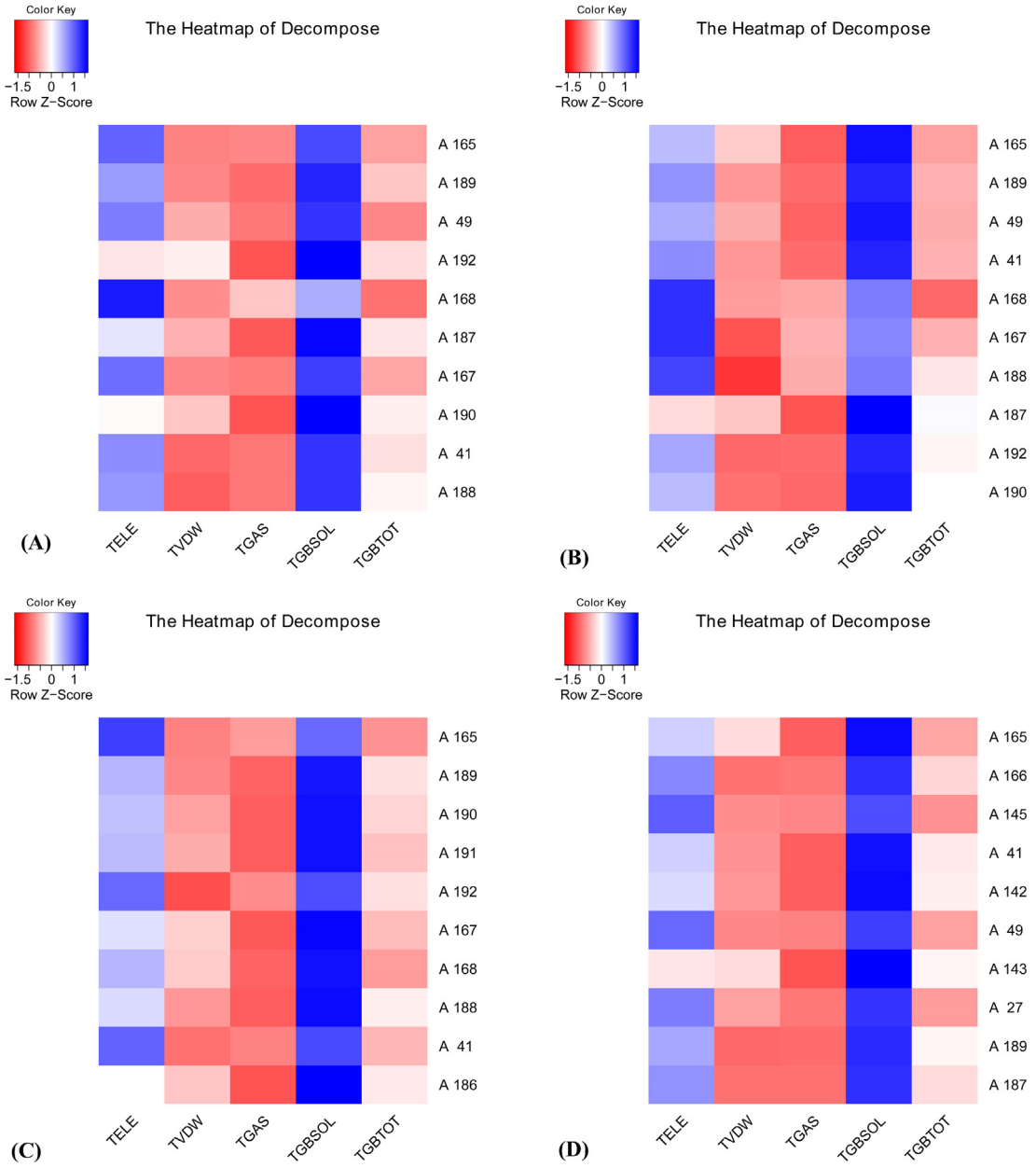

Fig. 9. Binding energy decomposition heatmap showing the major residues contributing to the total binding free energy.

M (Lockbaum et al., 2021). We have used 21 phytochemicals belonging to class Flavonoids, essential oils and polyphenols and screened these phytochemicals for their oral bioavailability. The filtered drug-like molecules were studied for their ability to bind and interact with the target enzyme. The best three molecules interacting with the target enzyme were identified to be Alpinetin, Pinocembrin and Pinostrobin which were held to the binding pocket with hydrogen bonds and hydrophobic interactions. Interestingly, His41 and Cys145, which constitute a catalytic dyad, are also observed interacting with the molecules. The dynamic behaviour of the protein–ligand complexes was studied using 100 ns MD simulations and their stabilities were confirmed in terms of RMSD, Rg, SASA and number of hydrogen bonds. While covalent inhibitors of SARS-CoV-2 main protease have shown great potency and effectiveness, non-covalent inhibitors of the enzyme are lacking. Our results have shown the prospect of the active components of *B. rotunda* through non-covalent inhibition of SARS-CoV-2 main protease. While the results are promising, further wet-lab experimentations are needed to confirm the anti-SARS-CoV-2 activity of the compounds. It would be also interesting to explore the effectiveness of these phytochemicals against the new emerging strains of coronaviruses to develop into broad-spectrum inhibitors.

5. Conclusion

The lack of effective therapeutic drugs against SARS-CoV-2 infections and the continued rise in the fatality rate warrant the identification of novel drug candidate molecules. SARS-CoV-2 M^{pro} is a validated drug target involved in the maturation and cleavage of polyproteins during viral replication. In our study, we have explored the potential of major active phytochemicals of a *B. rotunda*, a perennial herb of immense tremendous medicinal properties using a combined approach of molecular docking and dynamics simulation. We identified three active flavonoids – Alpinetin, Pinocembrin and Pinostrobin which exhibit high binding affinities to the drug target receptor. Wet-lab experimentations

are needed to confirm the current findings before they may be developed into anti-SARS-CoV-2 therapeutic candidate molecules.

Declaration of Competing Interest

The authors declare that they have no known competing financial interests or personal relationships that could have appeared to influence the work reported in this paper.

Acknowledgments

The authors would like to extend their sincere appreciation to the Researchers Supporting Project number (RSP-2021/306), King Saud University, Riyadh, Saudi Arabia.

References

Abdelwahab, S.I., Mohan, S., Abdulla, M.A., Sukari, M.A., Abdul, A.B., Taha, M.M.E., Syam, S., Ahmad, S., Lee, K.-H., 2011. The methanolic extract of Boesenbergia rotunda (L.) Mansf. and its major compound pinostrobin induces anti-ulcerogenic property in vivo: possible involvement of indirect antioxidant action. J. Ethnopharmacol. 137 (2), 963–970.

Anand, K., Ziebuhr, J., Wadhwani, P., Mesters, J.R., Hilgenfeld, R., 2003. Coronavirus main proteinase (3CLpro) structure: basis for design of anti-SARS drugs. Science (80-.) 300 (5626), 1763–1767.

Bhamarapravati, S., Juthapruth, S., Mahachai, W., Mahady, G., et al., 2006. Antibacterial activity of Boesenbergia rotunda (L.) Mansf. and Myristica fragrans Houtt. against Helicobacter pylori. Songklanakarin J. Sci. Technol. 28, 157–163.

Chan, J.-W., Kok, K.-H., Zhu, Z., Chu, H., To, K.-W., Yuan, S., Yuen, K.-Y., 2020. Genomic characterization of the 2019 novel human-pathogenic coronavirus isolated from a patient with atypical pneumonia after visiting Wuhan. Emerg. Microbes Infect. 9 (1), 221–236.

Chander, M.P., Vinod Kumar, K., Lall, C., Vimal Raj, R., Vijayachari, P., 2016. GC/MS profiling, in vitro anti-leptospiral and haemolytic activities of Boesenbergia rotunda (L.) Mansf. used as a medicinal plant by Nicobarese of Andaman and Nicobar Islands. Nat. Prod. Res. 30 (10), 1190–1192.

Cheah, S.-C., Appleton, D.R., Lee, S.-T., Lam, M.-L., Hadi, A.H.A., Mustafa, M., et al., 2011. Panduratin A inhibits the growth of A549 cells through induction of apoptosis and inhibition of NF-KappaB translocation. Molecules 16, 2583–2598.

Chee, C.F., Abdullah, I., Buckle, M.J.C., Abd Rahman, N., 2010. An efficient synthesis of ($\pm$)-panduratin A and ($\pm$)-isopanduratin A, inhibitors of dengue-2 viral activity. Tetrahedron Lett. 51, 495–498.

Chen, N., Zhou, M., Dong, X., Qu, J., Gong, F., Han, Y., Qiu, Y., Wang, J., Liu, Y., Wei, Y., Xia, J., Yu, T., Zhang, X., Zhang, L.i., 2020. Epidemiological and clinical characteristics of 99 cases of 2019 novel coronavirus pneumonia in Wuhan, China: a descriptive study. Lancet 395 (10223), 507–513.

Chiang, M., Kurmoo, Y., Khoo, T.-J., 2017. Chemical-and cell-based antioxidant capacity of methanolic extracts of three commonly edible plants from Zingiberaceae family. Free Radicals Antioxidants 7 (1), 57–62.

Eng-Chong, T., Yean-Kee, L., Chin-Fei, C., Choon-Han, H., Sher-Ming, W., Li-Ping, C.T., Gen-Teck, F., Khalid, N., Abd Rahman, N., Karsani, S.A., et al., 2012. Boesenbergia rotunda: from ethnomedicine to drug discovery Evidence-Based Complement. Altern. Med. 2012.

Gurung, A.B., Bhattacharjee, A., Ali, M.A., 2016. Exploring the physicochemical profile and the binding patterns of selected novel anticancer Himalayan plant derived active compounds with macromolecular targets. Informatics Med. Unlocked 5, 1–14.

Halgren, T.A., 1996. Merck molecular force field. I. Basis, form, scope, parameterization, and performance of MMFF94. J. Comput. Chem. 17, 490–519. https://doi.org/10.1002/(SICI)1096-987X(199604)17:5/6<490::AID-JCC1>3.0.CO;2-P.

Hao, G.-F., Zhu, X.-L., Ji, F.-Q., Zhang, L.i., Yang, G.-F., Zhan, C.-G., 2009. Understanding the mechanism of drug resistance due to a codon deletion in protoporphyrinogen oxidase through computational modeling. J. Phys. Chem. B 113 (14), 4865–4875.

Hess, B., Kutzner, C., Van Der Spoel, D., Lindahl, E., 2008. GRGMACS 4: Algorithms for highly efficient, load-balanced, and scalable molecular simulation. J. Chem. Theory Comput. 4, 435–447. https://doi.org/10.1021/ct700301q.

Hilgenfeld, R., 2014. From SARS to MERS: crystallographic studies on coronaviral proteases enable antiviral drug design. FEBS J. 281 (18), 4085–4096.

Hou, T., Wang, J., Li, Y., Wang, W., 2011. Assessing the performance of the MM/PBSA and MM/GBSA methods. 1. The accuracy of binding free energy calculations based on molecular dynamics simulations. J. Chem. Inf. Model. 51 (1), 69–82.

Hu, B., Guo, H., Zhou, P., Shi, Z.-L., 2020. Characteristics of SARS-CoV-2 and COVID-19. Nat. Rev. Microbiol. 19 (3), 141–154.

Isa, N.M., Abdelwahab, S.I., Mohan, S., Abdul, A.B., Sukari, M.A., Taha, M.M.E., Syam, S., Narrima, P., Cheah, S.C., Ahmad, S., Mustafa, M.R., 2012. In vitro anti-inflammatory, cytotoxic and antioxidant activities of boesenbergin A, a chalcone isolated from Boesenbergia rotunda (L.)(fingerroot). Brazilian J. Med. Biol. Res. 45 (6), 524–530.

Kanjanasirirat, P., Suksatu, A., Manopwisedjaroen, S., Munyoo, B., Tuchinda, P., Jearawuttanakul, K., Seemakhan, S., Charoensutthivarakul, S., Wongtrakoongate, P., Rangkasenee, N., Pitiporn, S., Waranuch, N., Chabang, N., Khemawoot, P., Sangiamsuntorn, K., Pewkliang, Y., Thongsri, P., Chutipongtanate, S., Hongeng, S., Borwornpinyo, S., Thitithanyanont, A., 2020. High-content screening of Thai medicinal plants reveals Boesenbergia rotunda extract and its component Panduratin A as anti-SARS-CoV-2 agents. Sci. Rep. 10 (1). https://doi.org/10.1038/s41598-020-77003-3.

Kiat, T.S., Pippen, R., Yusof, R., Ibrahim, H., Khalid, N., Rahman, N.A., 2006. Inhibitory activity of cyclohexenyl chalcone derivatives and flavonoids of fingerroot, Boesenbergia rotunda (L.), towards dengue-2 virus NS3 protease. Bioorganic \& Med. Chem. Lett. 16 (12), 3337–3340.

Kim, S., Thiessen, P.A., Bolton, E.E., Chen, J., Fu, G., Gindulyte, A., Han, L., He, J., He, S., Shoemaker, B.A., Wang, J., Yu, B.o., Zhang, J., Bryant, S.H., 2016. PubChem Substance and Compound databases. Nucleic Acids Res. 44 (D1), D1202–D1213. https://doi.org/10.1093/nar/gkv951.

Laskowski, R.A., Swindells, M.B., 2011. LigPlot+: multiple ligand-protein interaction diagrams for drug discovery. J. Chem. Inf. Model. 51 (10), 2778–2786. https://doi.org/10.1021/ci200227u.

Lipinski, C.A., 2004. Lead- and drug-like compounds: the rule-of-five revolution. Drug Discov. Today. Technol. 1 (4), 337–341. https://doi.org/10.1016/j.ddtec.2004.11.007.

Lockbaum, G.J., Reyes, A.C., Lee, J.M., Tilvawala, R., Nalivaika, E.A., Ali, A., Kurt Yilmaz, N., Thompson, P.R., Schiffer, C.A., 2021. Crystal structure of SARS-CoV-2 main protease in complex with the non-covalent inhibitor ML188. Viruses 13 (2), 174. https://doi.org/10.3390/v13020174.

Lu, R., Zhao, X., Li, J., Niu, P., Yang, B.o., Wu, H., Wang, W., Song, H., Huang, B., Zhu, N. a., Bi, Y., Ma, X., Zhan, F., Wang, L., Hu, T., Zhou, H., Hu, Z., Zhou, W., Zhao, L.i., Chen, J., Meng, Y., Wang, J.i., Lin, Y., Yuan, J., Xie, Z., Ma, J., Liu, W.J., Wang, D., Xu, W., Holmes, E.C., Gao, G.F., Wu, G., Chen, W., Shi, W., Tan, W., 2020. Genomic characterisation and epidemiology of 2019 novel coronavirus: implications for virus origins and receptor binding. Lancet 395 (10224), 565–574.

Madaka, F., Tewtrakul, S., et al., 2011. Anti-allergic activity of some selected plants in the genus Boesenbergia and Kaempferia. Sonklanakarin J. Sci. Technol. 33, 301.

Mahmood, A.A., Mariod, A.A., Abdelwahab, S.I., Ismail, S., Al-Bayaty, F., 2010. Potential activity of ethanolic extract of Boesenbergia rotunda (L.) rhizomes extract in accelerating wound healing in rats. J. Med. Plants Res. 4, 1570–1576.

Mengist, H.M., Dilnessa, T., Jin, T., 2021. Structural basis of potential inhibitors targeting SARS-CoV-2 main protease. Front. Chem., 9

Morris, G.M., Huey, R., Lindstrom, W., Sanner, M.F., Belew, R.K., Goodsell, D.S., Olson, A.J., 2009. AutoDock4 and AutoDockTools4: Automated docking with selective receptor flexibility. J. Comput. Chem. 30 (16), 2785–2791. https://doi.org/10.1002/jcc.v30:1610.1002/jcc.21256.

Ongwisespaiboon, O., Jiraungkoorskul, W., 2017. Fingerroot, Boesenbergia rotunda and its aphrodisiac activity. Pharmacogn. Rev. 11 (21), 27. https://doi.org/10.4103/phrev.phrev_50_16.

Pan, Y., Gao, D., Zhan, C.-G., 2008. Modeling the catalysis of anti-cocaine catalytic antibody: competing reaction pathways and free energy barriers. J. Am. Chem. Soc. 130 (15), 5140–5149.

Sander, T., Freyss, J., von Korff, M., Rufener, C., 2015. DataWarrior: an open-source program for chemistry aware data visualization and analysis. J. Chem. Inf. Model. 55 (2), 460–473. https://doi.org/10.1021/ci500588j.

Schüttelkopf, A.W., van Aalten, D.M.F., 2004. PRODRG: a tool for high-throughput crystallography of protein–ligand complexes. Acta Crystallogr. Sect. D Biol. Crystallogr. 60 (8), 1355–1363.

Udomthanadech, K., Vajrodaya, S., Paisooksantivatana, Y., 2015. Antibacterial properties of the extracts from some Zingibereous species in Thailand against bacteria causing diarrhea and food poisoning in human. Int. Trans. J. Eng. Manag. Appl. Sci. Technol. 6, 203–213.

Veber, D.F., Johnson, S.R., Cheng, H.-Y., Smith, B.R., Ward, K.W., Kopple, K.D., 2002. Molecular properties that influence the oral bioavailability of drug candidates. J. Med. Chem. 45 (12), 2615–2623.

Wu, N., Kong, Y.u., Zu, Y., Fu, Y., Liu, Z., Meng, R., Liu, X., Efferth, T., 2011. Activity investigation of pinostrobin towards herpes simplex virus-1 as determined by atomic force microscopy. Phytomedicine 18 (2-3), 110–118.

Zainin, N.S., Lau, K.Y., Zakaria, M., Son, R., Razis, A.F.A., Rukayadi, Y., 2013. Antibacterial activity of Boesenbergia rotunda (L.) Mansf. A. extract against Escherichia coli. Int. Food Res. J. 20, 3319.

Zhang, L., Lin, D., Sun, X., Curth, U., Drosten, C., Sauerhering, L., Becker, S., Rox, K., Hilgenfeld, R., 2020. Crystal structure of SARS-CoV-2 main protease provides a basis for design of improved α-ketoamide inhibitors. Science 368 (6489), 409–412. https://doi.org/10.1126/science:abb3405.

Ziebuhr, J., Snijder, E.J., Gorbalenya, A.E., 2000. Virus-encoded proteinases and proteolytic processing in the Nidovirales. J. Gen. Virol. 81, 853–879.